Journal of Solid State Chemistry 186 (2012) 109–115

Contents lists available at SciVerse ScienceDirect

Journal of Solid State Chemistry

journal homepage: www.elsevier.com/locate/jssc

Preparation and thermoelectric properties of ternary superionic conductor $CuCrS_2$

Yue-Xing Chen, Bo-Ping Zhang*, Zhen-Hua Ge, Peng-Peng Shang

School of Materials Science and Engineering, University of Science and Technology Beijing, No. 30 Xueyuan Road, Haidian Zone, Beijing 100083, PR China

ARTICLE INFO

Article history:
Received 4 August 2011
Received in revised form
21 November 2011
Accepted 26 November 2011
Available online 9 December 2011

Keywords:
Thermoelectric material
$CuCrS_2$
MA–SPS

ABSTRACT

Transition metal chalcogenide $CuCrS_2$ powder was synthesized by mechanical alloying (MA) and then consolidated by spark plasma sintering (SPS) technique at 673–1073 K. The phase structure, microstructure and thermoelectric properties of samples were characterized by X-ray diffraction (XRD), field emission scanning electron microscopy (FESEM) and Seebeck coefficient/electrical conductivity measuring system, respectively. All the bulks indicated a single phase $CuCrS_2$, while the high relative density over 90% were attained for the samples sintered at 873–1073 K. The electrical conductivity of bulk samples displayed a typical characteristic of semiconductor. With increasing measuring temperature, the conductive behaviour of bulk samples sintered over 973 K showed a semiconductor transformation from *n*-type to *p*-type due to the changes of main carrier type. The sample obtained by applying SPS at 873 K got the highest power factor 83.2 $\mu W\,m^{-1}\,K^{-2}$, and the largest *ZT* value 0.11 at 673 K.

1. Introduction

Ternary copper–chromium–sulfide $CuCrS_2$ belongs to the chalcogenide alloys of transition and monovalent metals AMX_2 (A=Cu or Ag; M=Cr, V, Ti or Mn; X=S, Se, or Te) which are layered materials with a hexagonal crystal system [1,2]. Recently, $CuCrS_2$ has attracted more and more attentions because it is a magnetic semiconductor at low temperature and a superionic conductor at high temperature [3]. The $CuCrS_2$ consists of alternating S–Cr–S triple-atomic layers structure perpendicular to the hexagonal *c*-axis, in which the copper ions occupy half of tetrahedral interstice between every two layers [4–6]. The atoms inside the triple layers of CrS_2 are bound to each other by strong ionic bonds, while the neighboring triple layers are bound to each other by weak van der Waals forces. It reveals that Cu ions with a high ionic conductivity are not strongly bonded with the CrS_2 layers. According to Engelsman's reports [7], the sublattice of Cu ions consists of two sublattices α and β. At room temperature only α sublattice is occupied, while both α and β sublattices above the phase transition temperature (675 K) are occupied with equal probability, which leads to rise in the electrical properties of $CuCrS_2$ simultaneously [8,9]. The electrical properties of $CuCrS_2$ were measured by Nagard et al. [3], which indicated that $CuCrS_2$ has a semiconductor conductive behavior. The electrical conductivity of $CuCrS_2$ spans several orders of magnitude by different methods. $CuCrS_2$ characterizes a mixed conductor with ion conductivity and electronic conductivity in the same time and shows an electrical conductivity of about 10^{-4} S/cm at low temperature (below 300 K) [10–12]. Tewari et al. [13] investigated recently thermoelectric properties of a $CuCrS_2$ sample obtained by a specific quench method with *c*-axis orientation and found that the electrical conductivity and Seebeck coefficient at room temperature (300 K) were 1.67×10^3 S/cm and 445 $\mu V\,K^{-1}$, respectively. The specific heat treat process makes the sample to have a highly textured structure, which lead to the mutation of sample's electrical properties. However, the temperature dependence of the thermoelectric properties of $CuCrS_2$ has not been well investigated so far. There is sufficient room to regulate the electrical transport properties of $CuCrS_2$ by different methods.

Compared to the traditional solid state sintering, mechanical alloying (MA) combining spark plasma sintering (SPS) technique was used to prepare bulk materials with fine grains and dense microstructure, which are obvious benefit to the thermoelectric property of materials. In this study, $CuCrS_2$ bulk materials were prepared by SPS technique using MA treated powders. The microstructure and electrical transport properties of $CuCrS_2$ were investigated with a special emphasis on the influence of SPS temperature. The peak *ZT* value is 0.11 at 673 K for the sample sintered at 873 K, whose power factor and thermal conductivity at 673 K are 83.2 $\mu W\,K^{-2}\,m^{-1}$ and 0.53 $W\,m^{-1}\,K^{-1}$, respectively.

2. Experimental

Elements Cu (99.9%), Cr (99.9%) and S (99.5%) were subjected to MA according to the molar ratio with a formula of $CuCrS_2$ using

* Corresponding author.
E-mail address: sendaimr@gmail.com (B.-P. Zhang).

0022-4596/$ - see front matter © 2011 Elsevier Inc. All rights reserved.
doi:10.1016/j.jssc.2011.11.040

a planetary ball mill (QM-4F, Nanjing University, China) at 425 rpm for different hours in a purified argon atmosphere. Stainless steel vessels and balls were used. The weight ratio of ball to powder was kept at 20:1. Subsequently, the MA-treated powders at 425 rpm for 40 h were sintered under an axial compressive pressure of 40 MPa at 673, 773, 873, 973 and 1023 K using a SPS system (Sumitomo SPS1050, Japan). The heating rate and the holding time were 100 K min^{-1} and 5 min, respectively. Finally, a disk-shaped sample with a dimension of Φ 20 mm × 4 mm was obtained. The density of sintered samples was measured by the Archimedes method.

Phase structure was analyzed by X-ray diffraction (XRD, Cu$K\alpha$, BrukerD8, Germany). The morphologies of fractographs and energy dispersive spectrum (EDS) of bulks were investigated by a field emission scanning electron microscopy (FESEM, SUPRATM 55, Germany). The Seebeck coefficient and electrical conductivity were measured from 323 to 623 K using a Seebeck coefficient/electrical conductivity measuring system (ZEM-2, Ulvac-Riko, Japan) in a helium atmosphere. The thermal diffusivity coefficient (D) was measured using the laser flash method (NETZSCH, LFA427, Germany). The specific heat (C_p) was measured using a thermal analyzing apparatus (Dupont 1090B, USA). The density (d) of the sample was measured by the Archimedes method. The thermal conductivity (κ) was calculated from the product of thermal diffusivity, specific heat (C_p) and density, $\kappa = DC_pd$. The Hall coefficient (R_H) of the samples was measured at 323 K using a physical properties measurement system (PPMS-9T, Quantum Design Inc., USA), in which a magnetic field of 2 T and an electric current of 30 mA were applied for the measurements.

3. Results and discussion

Fig. 1 shows XRD patterns of the powders subjected to MA at 425 rpm for different hours. Three phases including CuS (PDF#06-0464), Cr (PDF#85-1335) and S (PDF#08-0247) are detected from the XRD pattern for the sample after applying MA for 28 h, which indicates that the CuS phase with a hexagonal symmetry is easily formed. Prolonging the ball milling time to 36 h leads to forming CuS_2 phase with a cubic crystal symmetry, while the Cr phase still exists in the powder at this MA stage. The XRD pattern of the powder after ball milling for 40 h is well-matched with the standard card of $CuCrS_2$ (PDF#23-0952), which indicates the formation of a single $CuCrS_2$ phase with a rhombohedral symmetry. No skewing behavior is observed for the main diffraction peaks of (101), (107), (018) and (110). The broadened diffraction peaks after ball milling for over 40 h indicate that the MA-treated $CuCrS_2$ power is very fine and has a low degree of crystallization, which are in favor of enhancing TE properties.

Fig. 2 shows the XRD patterns of the $CuCrS_2$ bulks sintered at different temperatures by using the MA-treated powder at 425 rpm for 40 h. All the characteristic peaks coincide well with those of $CuCrS_2$ (PDF#65-2098), indicating that the sintered bulks maintain the single-phase structure of $CuCrS_2$ at 673–1073 K. The enlarged diffraction peaks of the (101), (107), (018) and (110) in different 2-theta ranges for the samples are shown in Fig. 3. Judging from the figure, all the diffraction peaks of samples sintered at low temperatures (673, 773 and 873 K) coincide well with those of standard card of $CuCrS_2$ (PDF#23-0952) without an obvious skewing behavior. As raising the sintering temperature to 973 and 1073 K, the (101), (107), (018) and (110) peaks all show an obvious shift to low diffraction angles, in which the offset of diffraction peaks (107) and (110) is about 0.25° and 0.24°, respectively. This means that the resultant samples undergo an obvious increase in the lattice parameters and a tiny variation on the composition. Sulfur has a low melting point about 385 K,

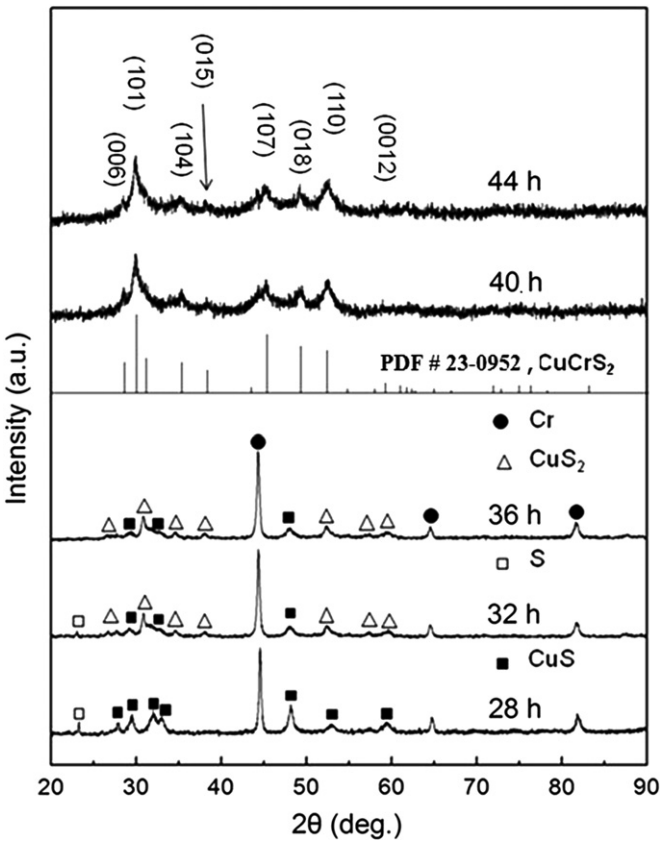

Fig. 1. XRD patterns of the $CuCrS_2$ powders subjected to MA at 425 rpm for different hours.

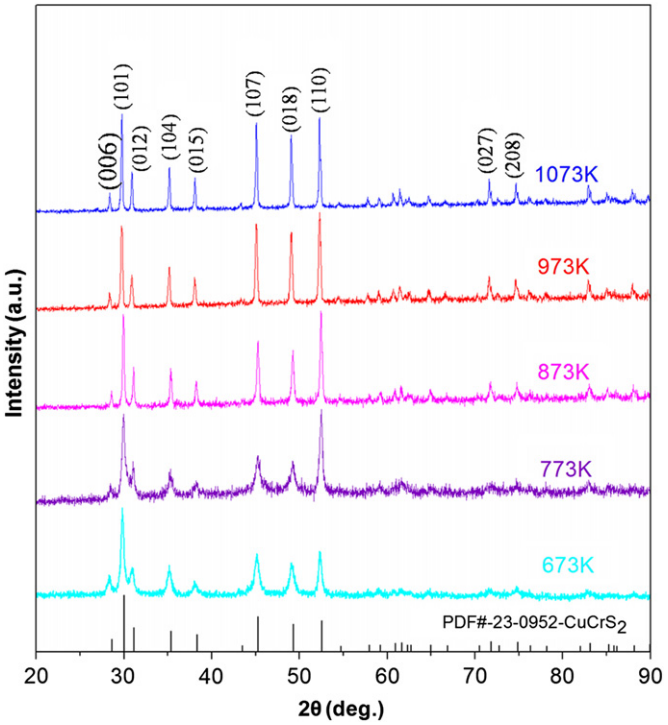

Fig. 2. XRD patterns of the $CuCrS_2$ bulks the $CuCrS_2$ bulks obtained by applying SPS for 5 min at different temperatures.

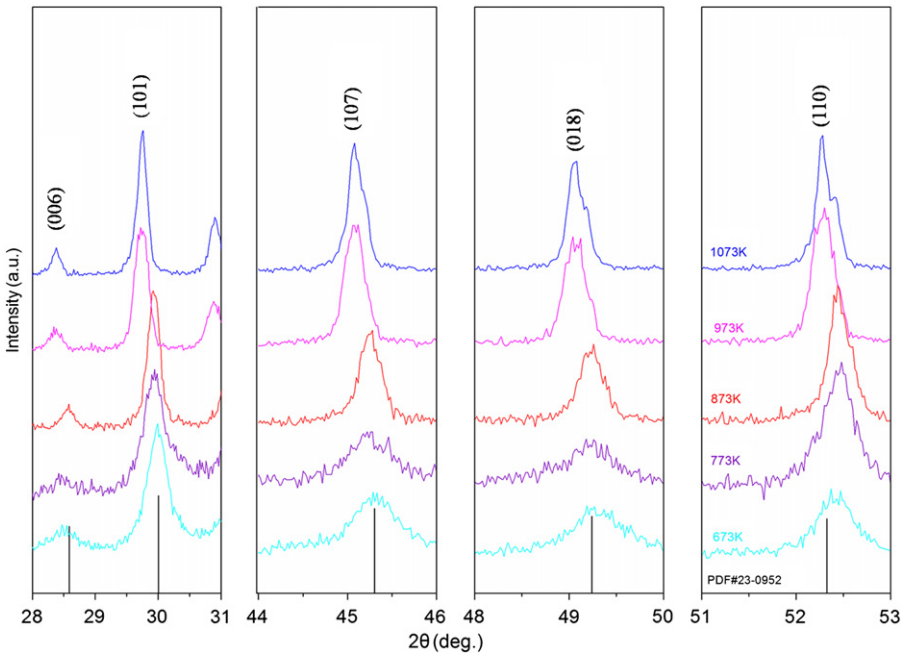

Fig. 3. XRD patterns in different 2 theta ranges of the $CuCrS_2$ bulks obtained by applying SPS for 5 min at different temperatures.

a part of sulfur may go out of lattice structure via the volatilization due to the excessive high temperature during the SPS process. As a result the diffraction peaks shifted to low angles which led to increase lattice constants. As calculated by the EDS data, the S/(Cu+Cr) atom ratio of $CuCrS_2$ samples sintered at 673, 773, 873, 973 and 1073 K are 93.59%, 93.05%, 92.94%, 91.09% and 90.44%, respectively, indicating that the S volatilization increases with increasing sintering temperature. The same shift behavior of the 2θ angles towards lower diffraction angle was also observed in Bi_2S_3 bulk samples with raising SPS temperature [14,15]. The X-ray fluorescence (XRF) measurement of the corresponding Bi_2S_3 bulk samples indicated that the ratio of Bi to S decreases as the 2θ angles shift to low angles [15]. The present fact is also consistent with the result [16] that the chemical composition of $CuCrS_2$ varies from $CuCrS_2$ at 873 K to $CuCrS_{1.92}$ when the temperature raised to 1273 K, indicating that sulfur deficiency is prevalent in $CuCrS_2$ structure at high temperature. XRD peaks become gradually sharper with increasing sintering temperature, suggesting that the samples sintered at high temperatures have a higher degree of crystallization and larger size grains.

Fig. 4 shows the FESEM micrographs of the fractured surfaces for $CuCrS_2$ bulks sintered at different temperatures. Many interstices in Fig. 4(a) and (b) exist in the bulks sintered at 673 and 773 K, which shows a loosened microstructure with small granular grains about 200–500 nm in an average diameter. The grain size of bulks sintered above 873 K grows to about 1–1.5 μm with raising sintering temperature. At the same time, a lot of pores are observed in Fig. 4(d) and (e) for the samples sintered at 973 and 1073 K which is due to the volatilization of sulfur during the SPS process.

Table 1 lists the sintering conditions, densities, Hall coefficient, carrier concentration and mobility of $CuCrS_2$ samples sintered at different temperatures. The relative density of sample sintered at 673 K is 70.1%, and increases to 75.1%, 94.6% and 95.7% for the samples sintered at 773, 873 and 973 K, respectively. The carrier concentration (n) is calculated from the Hall coefficient data by the relationship

$$n = 1/R_H e \tag{1}$$

where R_H and e are Hall coefficient and the electron charge, respectively. The carrier concentration of the sample sintered at 773 K under 40 MPa is $5.09\times10^{14}\ cm^{-3}$. As rising the sintering temperature to 973 K, the carrier concentration was decreased rapidly to a low value of $1.2\times10^{13}\ cm^{-3}$. The decreased carrier concentration is attributed to the tiny variation of $CuCrS_2$ component with increasing SPS temperature, in which the (107) and (110) diffraction peaks of sample show an offset about 0.25° and 0.24° to low angles in XRD pattern (Fig. 3). This is because the sulfur vacancies ($V_s^{\bullet\bullet}$) generated in the crystal lattice caused by the volatilization of sulfur at high temperature leads to the increase of electron concentration. This process can be described by following defects equation:

$$CuCrS_{2-x} \rightarrow CuCrS_2 - xS\uparrow + xV_s^{\bullet\bullet} + 2xe' \tag{2}$$

Generated electrons during this process combine with the holes, which are the major carrier, to form electron–hole pairs making a great decrease in the carrier concentration of bulks. Hence, if the reaction of the defects Eq. (2) was accelerated by raising sintering temperature, a mass of the electrons would generate and make the major carrier likely changes to electron from hole, which could result in the conductive transition of p-type to n-type. The carrier mobility is calculated from the Hall coefficient data by the relationship:

$$\mu = R_H\sigma \tag{3}$$

where R_H, σ are the Hall coefficient and the electrical conductivity, respectively. As listed in Table 1, the carrier mobility increases from 140 to 984 $cm^2\ V^{-1}\ s^{-1}$ with increasing SPS temperature from 773 to 973 K, which is attributed to the densified microstructure and the grown grains.

Fig. 5 shows the temperature dependence of electrical transport properties for $CuCrS_2$ bulks obtained by applying SPS for 5 min at 673–1073 K. The electrical conductivity in Fig. 5(a) for the sample sintered at 673 K is 49.8–69.5 $S\ m^{-1}$ over the whole test coverage, which may due to its low relative density (70.1%). It is well known that electrical conductivity is proportional to carrier mobility and carrier concentration which refers

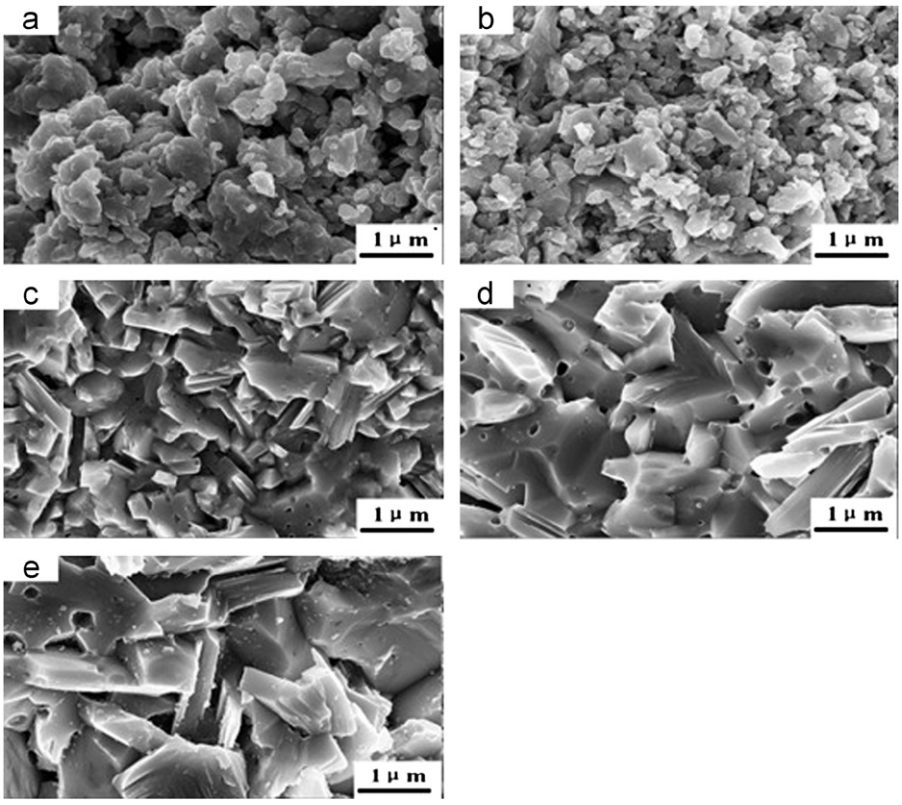

Fig. 4. FESEM micrographs of $CuCrS_2$ bulks obtained by applying SPS for 5 min at 673 K (a), 773 K (b), 873 K (c), 973 K (d) and 1073 K (e).

Table 1
Sintering conditions, densities, Hall coefficient, carrier concentration and mobility of $CuCrS_2$ bulk samples.

Sintering conditions		Measured density (g/cm^3)	Relative density (%)[a]	Hall coefficient R_H (10^4 cm^3/C)	Carrier concentration n ($10^{14}/cm^3$)	Carrier mobility μ ($cm^2/V\,s$)
Temperature (K)	Pressure (MPa)					
673	40	3.19	70.1	–	–	–
773	40	3.44	75.1	1.23	5.09	140
873	40	4.30	94.6	7.67	0.82	490
973	40	4.35	95.7	50.46	0.12	984
1073	40	4.36	95.8	–	–	–

[a] With regard to the theoretical density of 4.55 g/cm^3.

to following base equation:

$$\sigma = ne\mu \tag{4}$$

where σ, μ, n are electrical conductivity, carrier mobility, carrier concentration, respectively. Raising SPS temperature to 773 K leads to densify the microstructure and to grow grains, which increase the carrier mobility and make its electrical conductivity at room temperature almost twice higher than that of the sample sintered at 673 K. The electrical conductivities of samples sintered over 873 K all show a dramatic decline to less than 20 $S\,m^{-1}$ at 323 K which is due to the obvious decrease of carrier concentration (Table 1). It is noticed that the electrical conductivity of sample sintered at 873 K increases with measuring temperature, which shows an obvious semiconductor conducting behavior. The highest electrical conductivity is 490 $S\,m^{-1}$ at 673 K for the sample sintered at 873 K, which is three times more than that of sample sintered at 773 K. There are two main reasons to explain this fact. One is that the carrier mobility of bulk sintered at 873 K has greatly increased as listed in Table 1, which play a dominant impact than that of the decreased carrier concentration on the electrical conductivity with increasing testing temperature, finally make its electrical conductivity obviously higher than the bulks sintered at 673 and 773 K. The other is that a greatly enhancive ionic conductivity caused by the varied location of Cu ions in the crystal structure with raising temperature since $CuCrS_2$ is a superionic conductor, in which the Cu ions between the neighboring triple layers are bound to each another by weak van der Waals forces and exhibit a high mobility.[3] The sample sintered at 873 K have a higher Cu ions mobility than the other samples which exhibit a ions conductivity. However, the conductivity of samples decreases by further raising sintering temperature to 973 and 1073 K. This is because the sulfur vacancies ($V_S^{\bullet\bullet}$) generated in the crystal lattice become serious owing to the part volatilization of sulfur at the excessive temperature. During this process, the generated electrons combine with the holes and form the electron–hole pairs, which greatly decrease the carrier concentration of bulks. The greatly decreased carrier concentration becomes dominate to affect the electrical conductivity as the sintering temperature was over 873 K. To sum up, the low electrical conductivity of samples sintered at 673 K and 773 K is mostly attributed to the low carrier mobility which is due to their low dense microstructure and small size of grains. As to the samples

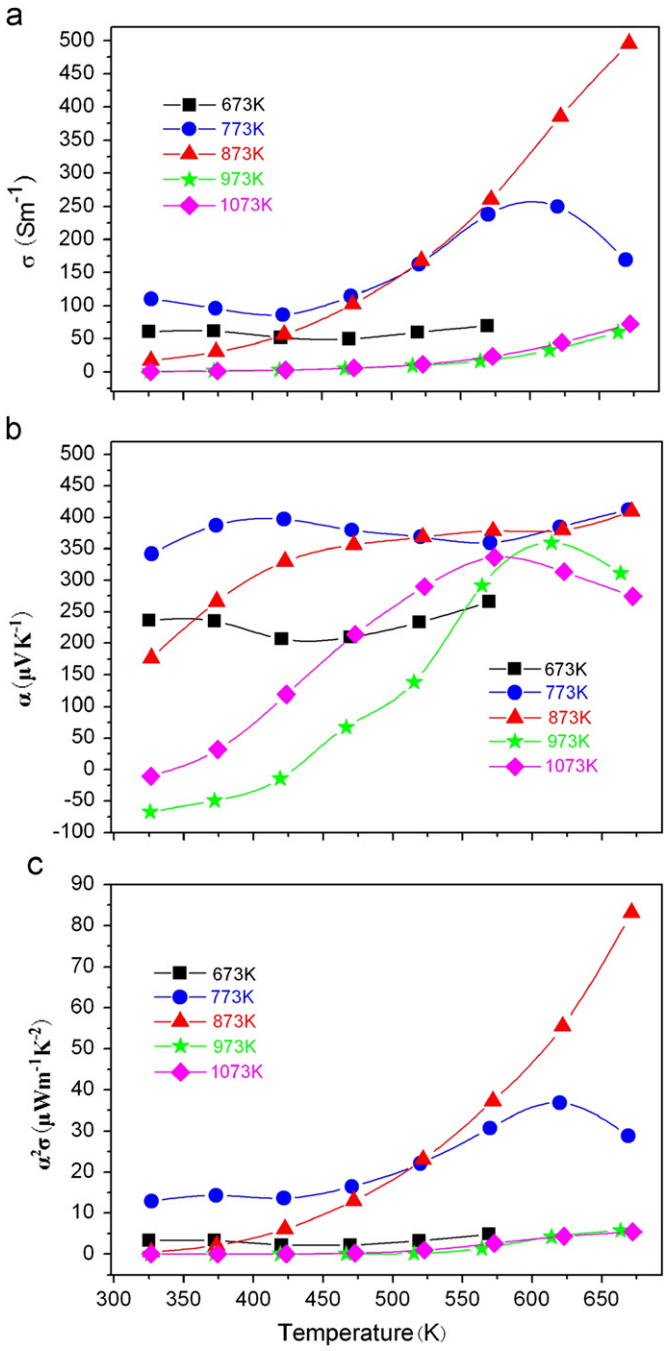

Fig. 5. Temperature dependence of electrical conductivity (a), Seebeck coefficient (b) and power factor (c) for $CuCrS_2$ bulks obtained by applying SPS for 5 min at 673–1073 K.

sintered over 873 K, the carrier concentration becomes the dominant factor of total electrical conductivity. The difference between the sample sintered at 873 K and ones at 973 and 1073 K is that the later have an extremely low carrier concentration which make their electrical conductivity have an unobvious increasing (from 0.5 S m^{-1} to 72.5 S m^{-1}) over the whole measuring temperature.

Fig. 5(b) shows the temperature dependence of Seebeck coefficients for samples sintered at different temperatures. The positive values of Seebeck coefficient indicate that the samples are *p*-type and the major carrier is holes. The Seebeck coefficient can refer to following equation:

$$S \approx \gamma - \ln n \quad (5)$$

where S, n and γ are Seebeck coefficient, carrier concentration and scattering factor, respectively. The Seebeck coefficient is inversely proportional to the carrier concentration and proportional to the scattering factor. The Seebeck coefficient of the sample sintered at 673 K display a slight fluctuate around 250 μV K^{-1}, while the sample sintered at 773 K exhibits a much higher S value about 350–400 μV K^{-1} over the whole test range . This may due to the decrease of carrier concentration and the increase of the density, both of them are benefiting to the Seebeck coefficient of samples. The relative density of the two samples are 70.1% and 75.1%, respectively, which means the scattering factors will not have remarkable change during the whole testing temperature. Therefore, the carrier concentration will rarely change during the measuring period because the testing temperature does not cover the intrinsic excitation temperature. These two reasons lead to the slight fluctuate of samples' Seebeck coefficient. In a general way, the Seebeck coefficient and electrical conductivity of material demonstrate an opposite trend with increasing temperature. However, for the samples sintered above 873 K (873, 973 and 1073 K), both of the Seebeck coefficient and electrical conductivity exhibit an increase tendency with increasing test temperature. This can be explained by that the mechanism of mix-conduction (electronic conduction and ionic conduction) for the $CuCrS_2$ display a complicated impact during the properties testing period.

As shown in Fig. 5(b), the value of Seebeck coefficient for samples sintered at 973 and 1073 K changes from negative to positive as a function of measuring temperature, which indicates a conductive transition from *n*-type to *p*-type. Following the defects Eq. (2), the reduced sulfur atom causes a rise of electron concentration and made it to be the major carrier from the hole. The holes concentration increases with increasing measuring temperature, whereby more and more electron–hole pairs generate and make finally the holes to be the major carrier, which accordingly results in that the value of Seebeck coefficient turn to positive as raising measuring temperature to 973 K. The transition temperature from *n*-type to *p*-type drops to about 323 K from nearly 473 K as raising sintering temperature from 973 K to 1073 K. As shown in Fig. 5(b), the Seebeck coefficient of sample sintered at 973 K is about 70 μV K^{-1} at 323 K, which expresses the difference between the γ and the ln n. Owing to the serious volatilization of sulfur, as described in defects Eq. (2), the electron concentration of sample sintered at 1073 K is higher than the sample sintered at 973 K though the carrier concentrations of the two samples are all at a very low level, which increases the ln n value of the sample sintered at 1073 K. Since the scattering factor γ rarely changes as increasing the temperature to 1073 K, the Seebeck coefficient is decided by ln n and γ near to zero at room temperature, which means the transition temperature from *n*-type to *p*-type is about 323 K.

Fig. 5(c) shows the temperature dependence of power factor for bulk samples sintered at different temperatures. The sample by applying SPS at 873 K has high values of electrical conductivity (490 S m^{-1}) and Seebeck coefficient (410 μV K^{-1}) at 673 K, which contributes to the highest power factor of 83.2 μV m^{-1} K^{-2}. Therefore, a low relative density and/or a nonstoichiometric state for the samples all result in a decline of electrical properties. To further enhancing electrical transport properties, the materials should have a high relative density and maintain stable component.

Fig. 6 shows the temperature dependence of heat transport properties for the bulk samples sintered at 773 K, 873 K and 973 K. All thermal conductivities in Fig. 6(a) of three samples display a decreasing trend with the measuring temperature. Specifically, the sample sintered at 773 K has the lowest thermal conductivity about 0.34–0.47 W m^{-1} K^{-1}. While the thermal conductivity of the samples sintered at 873 K and 973 K show

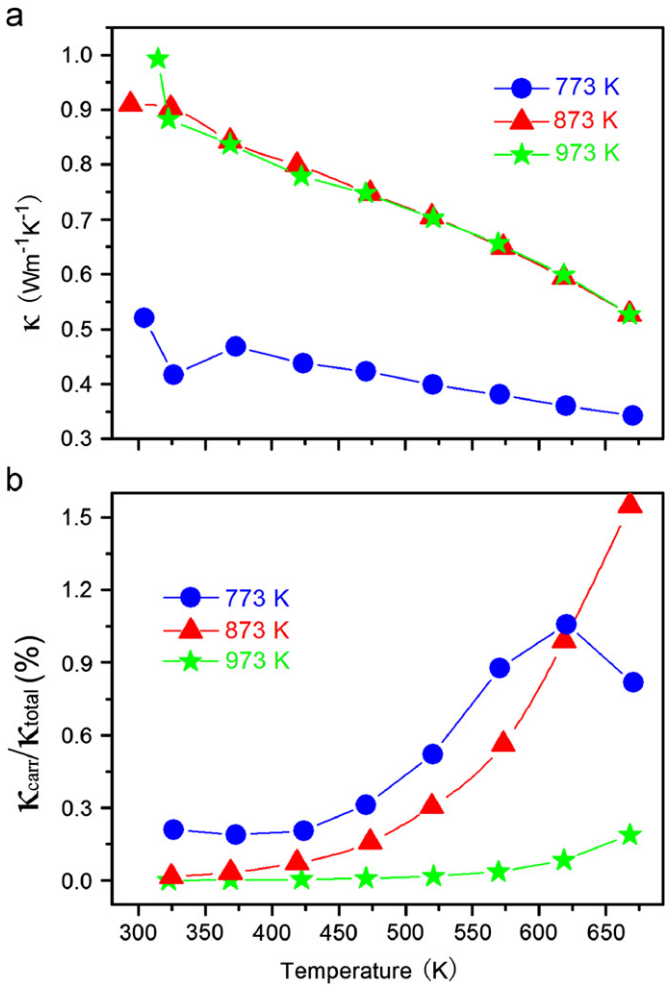

Fig. 6. Temperature dependence of thermal conductivity (a), the percentage of carrier thermal conductivity (b), for $CuCrS_2$ bulks obtained by applying SPS for 5 min at 773 K, 873 K and 973 K.

almost double value from 0.53 to 0.90 $W\,m^{-1}\,K^{-1}$ during the measuring temperature. Compared to the tradition thermoelectric material, the lower thermal conductivity of the $CuCrS_2$ may be originated from its special layered structure.

As well known, the thermal conductivity of material consists of carrier thermal conductivity and lattice thermal conductivity. The carrier thermal conductivity (κ_{carr}) can refer to following equation:

$$\kappa_{carr} = LT\sigma \tag{6}$$

where L, T and σ are Lorenz constant, absolute temperature and electrical conductivity, respectively. Fig. 6(b) shows the percentage of κ_{carr} for the bulk samples sintered at 773 K, 873 K and 973 K. The κ_{carr} of all the bulks displays an increasing trend as the function of measuring temperature, which consistent with the temperature dependence of the electrical conductivity as shown in Fig. 5(a), because both of them are proportional to the carrier mobility, carrier concentration and Hall coefficient. However, the κ_{carr} makes up less than 1.6% of thermal conductivity, even the κ_{carr} of sample sintered at 873 K that has an obvious rise than other samples. So the κ_{carr} of samples plays a less important role in thermal conductivity, and enhancing the electrical conductivity will not produce an evident change to sample's thermal conductivity.

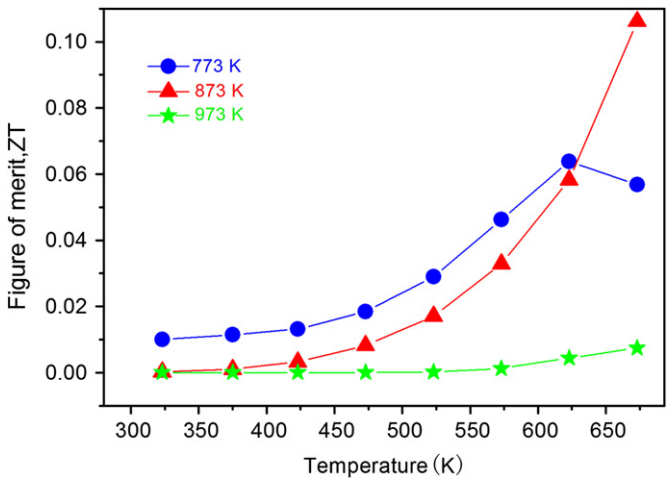

Fig. 7. Temperature dependence of ZT value for $CuCrS_2$ bulks obtained by applying SPS for 5 min at 773 K, 873 K and 973 K.

The lattice thermal conductivity ($\kappa_{lattice}$) can be calculated from the following relationship:

$$\kappa_{lattice} = \tfrac{1}{3} C_v V_s l \tag{7}$$

where C_v, V_s and l are constant-volume specific heat, diffusion average speed of phonons and mean free path, respectively. Fig. 6(c) shows the percentage of $\kappa_{lattice}$ for the bulk samples sintered at 773 K, 873 K and 973 K. Obviously, compared to the κ_{carr}, the $\kappa_{lattice}$ of samples have an opposite tendency as a function of measuring temperature, and play a dominant role in the total thermal conductivity of samples.

Owing to the low relative density and fine grains, the mean free path and diffusion average speed of phonons of the sample sintered at 773 K are in a low level, which finally make the thermal conductivity of the sample has a low value between 0.34 and 0.47 $W\,m^{-1}\,K^{-1}$. As to the samples sintered at 873 K and 973 K, the relative densities are higher and the grains are twice or three times larger than the sample sintered at 773 K, whereby the thermal conductivities are increased.

Fig. 7 shows the temperature dependence of ZT value for $CuCrS_2$ bulks obtained by applying SPS for 5 min at 773 K, 873 K and 973 K. All the ZT values of three samples increase as the function of measuring temperature. The highest ZT value reaches to 0.11 at 673 K for the sample sintered at 873 K, which is reported for the first time on middle temperature for this structure.

4. Conclusions

The single phase $CuCrS_2$ powder was synthesized by ball-milling at 425 rpm for 40 h. $CuCrS_2$ bulks with high relative density over 90% were fabricated by applying SPS techniques using MA-treated powders at 873–1073 K. The electrical conductivity of samples displays a typical characteristic of semiconductor as a function of temperature, in which the bulks sintered over 973 K show a semiconductor transformation from n-type to p-type as increasing testing temperature. The highest power factor reached 83.2 $\mu W\,m^{-1}\,K^{-2}$ at 673 K for the bulk sample sintered at 873 K, and the thermal conductivity of the sample was 0.53 $W\,m^{-1}\,K^{-1}$, whereby the ZT value of the sample was 0.11 at 673 K, which is reported for the first time on middle temperature for this structure. Adjusting composition and/or appropriately doping can be done to enhance the transport properties of material and increase the ZT value ultimately.

Acknowledgment

This work was supported by National Natural Science Foundation of China (Grant nos. 50972012 and 50820145203), High-Tech 863 Program of China (Grant no. 2009AA03Z216) and National Basic Research Program of China (Grant no. 2007CB607504).

References

[1] F.M.R. Engelsman, G.A. Wiegers, F. Jellinek, B. van Laar, J. Solid State Chem. 6 (1973) 574.
[2] A.G. Gerards, B.A. Boukamp, G.A. Wiegers, Solid State Ionics 9 (1983) 471.
[3] N. Le Nagard, G. Collin, Gorochov. Mat. Res. Bull. 14 (1979) 1411.
[4] T. Hibma, S. Strassler, Phys. Rev. B 28 (1983) 1002.
[5] K.D. Bronzema, G.A. Wiegers, Acta Cryst. B 38 (1982) 2229.
[6] T. Hibma, P. Bruesh, S. Strassler, Solid State Ionics 5 (1981) 481.
[7] F.M. Engelsmagn, A. Wiegersf, Jellinek, B. Laarj, Solid State Chem. 6 (1973) 574.
[8] R.F. Almukhametov, R.A. Yakshibaev, E.V. Gabitov, Fiz. Tverd. Tela 42 (2000) 1465.
[9] I.G. Vassilieva, T.Yu. Kardash, V.V. Malakhov, J. Struct. Chem. 50 (2009) 288.
[10] G.M. Abramova, A.M. Vorotynov, G.A. Petrakovaskii, Phys. Solid State 46 (2004) 2245.
[11] N. Tsujii, H. Kitazawa, G. Kido, Phys. Status Solidi 3 (2006) 2775.
[12] N. Tsujii, H. Kitazawa, J. Phys.: Condens. Matter 19 (2007) 145245.
[13] G.C. Tewari, T.S. Tripathi, A.K. Rastogi, J. Electron. Mater. 39 (2010) 1133.
[14] Z.H. Ge, B.P. Zhang, P.P. Shang, et al., J. Electron. Mater. 40 (2011) 1087.
[15] Z.H. Ge, B.P. Zhang, Z.X. Yu, et al., J. Mater. Res. 26 (2011) 2711.
[16] My. A. Boutbila, J. Rasneur, M. el Aatmani, H. Lyahyaoui, J. Alloys Compd. 244 (1996) 23.